Spatial and Temporal Variations in Coherence: A Velocity Map Across the Southern Alps, New Zealand

Jack McGrath[1]*, Dr John Elliott[1], Prof. Sandra Piazolo[1], Prof. Tim Wright[1], Dr Ian Hamling[2]

[1]University of Leeds, UK [2]GNS, Wellington, NZ

*Email: eejdm@leeds.ac.uk

70% of the deformation in central South Island caused by the continental transpression between the Australian and Pacific plates is accommodated by the Alpine Fault (AF) (Beavan et al., 2016). Although predominantly a strike-slip fault, the oblique relative plate motions result in 39 mm/yr fault parallel and 10 mm/yr fault perpendicular slip. This convergence has resulted in the rapid uplift of the Southern Alps. The launch of Sentinel-1 will allow measurements of ground motion at resolutions unattainable with GPS to ascertain heterogeneity of deformation, with the combination of ascending and descending tracks enabling vertical motions to be resolved. However, the Southern Alps are a difficult target, with their high relief resulting in spatially and temporally variable coherence due to challenging topography, high erosion rates , snow and glacial, and vegetated slopes.

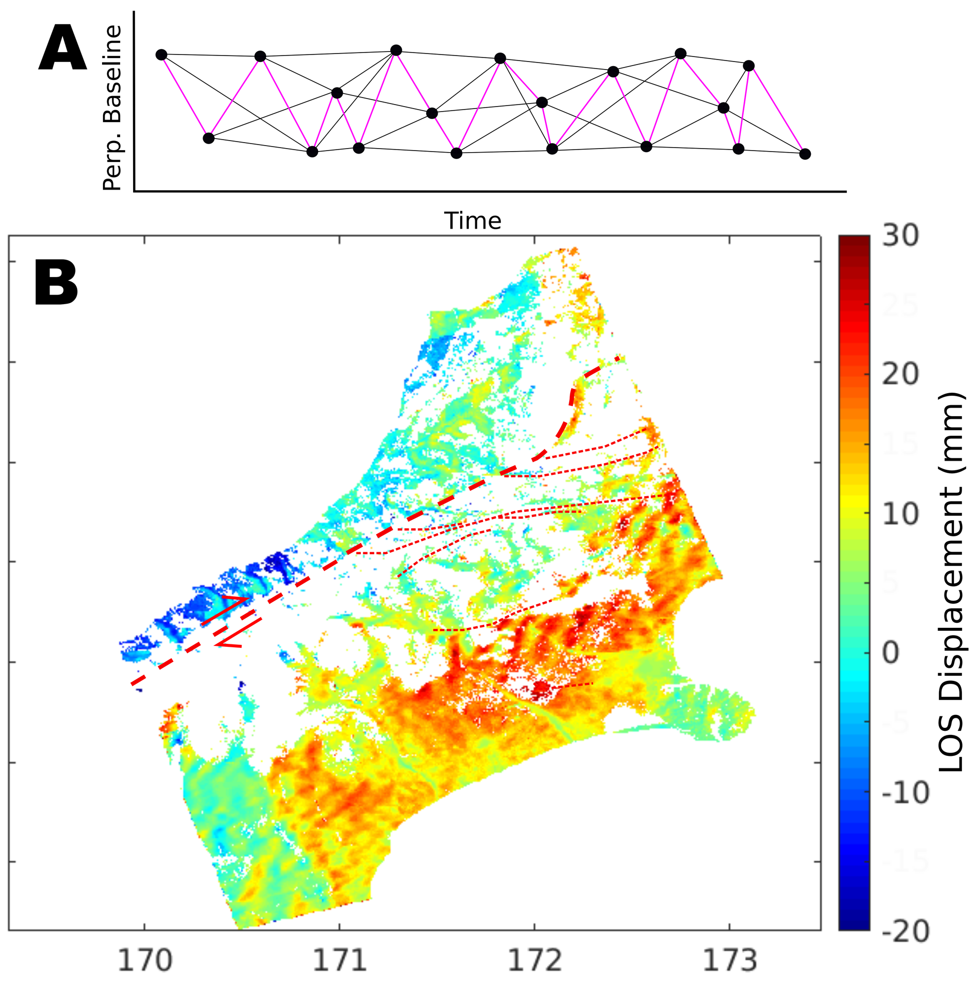

Fig 1) (A) 33 sequential 12-day interferograms (purple lines) of track 125A were taken from a network produced with the LiCSAR processor and chained together to provide total cumulative displacement over 2017.
(B) This results in a loss of signal near to the AF (thick dashed line), as well as larger LOS displacements from coast-to-coast than would be expected- in the near field the high incidence angle means only approximately half (~20 mm/yr) of displacement should be resolved in LOS.

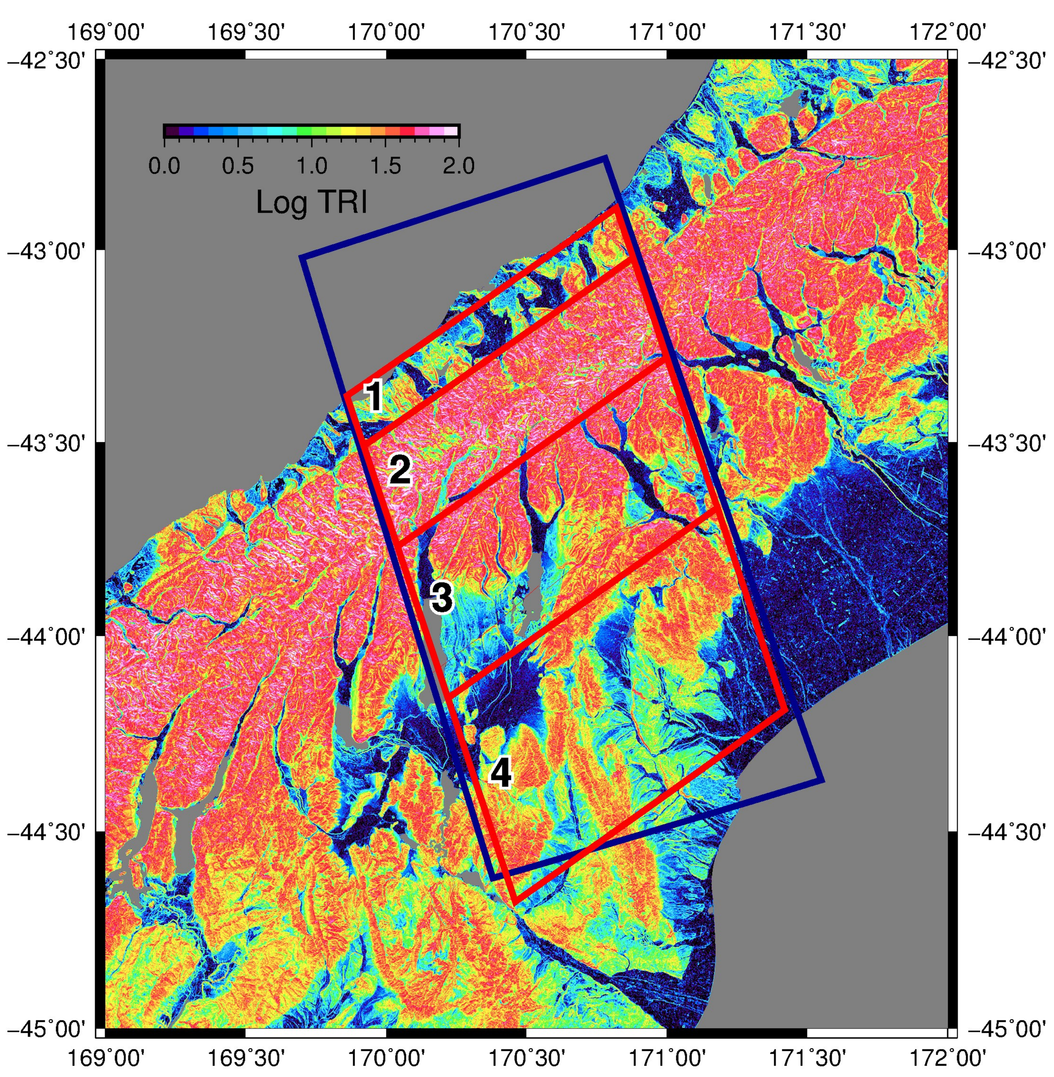

Fig 2) To see if the loss of data was due to coherence, the coherence across a single swath (blue box) was measured over the course of a year from 12, 24 and 36 day interferograms. To investigate spatial variations in topography, the swath was sub-divided into polygons defined by terrain ruggedness. The AF forms the boundary between between the Australian Plate and Southern Alps, and is clearly seen in the sharp change in ruggedness.
1) Australian Plate, 2) Southern Alps, 3) Southern Alps Foothills, 4) Canterbury Plain

Fig 3) The seasonal effect on coherence varies spatially. Higher summer coherence is seen in the areas of higher roughness (2 and 3), potentially due to increased snow cover during these periods. This demonstrates that it may be possible to create a continuous network of coherent interferograms over the Southern Alps with short temporal baselines in the summer and longer baselines spanning the winter.

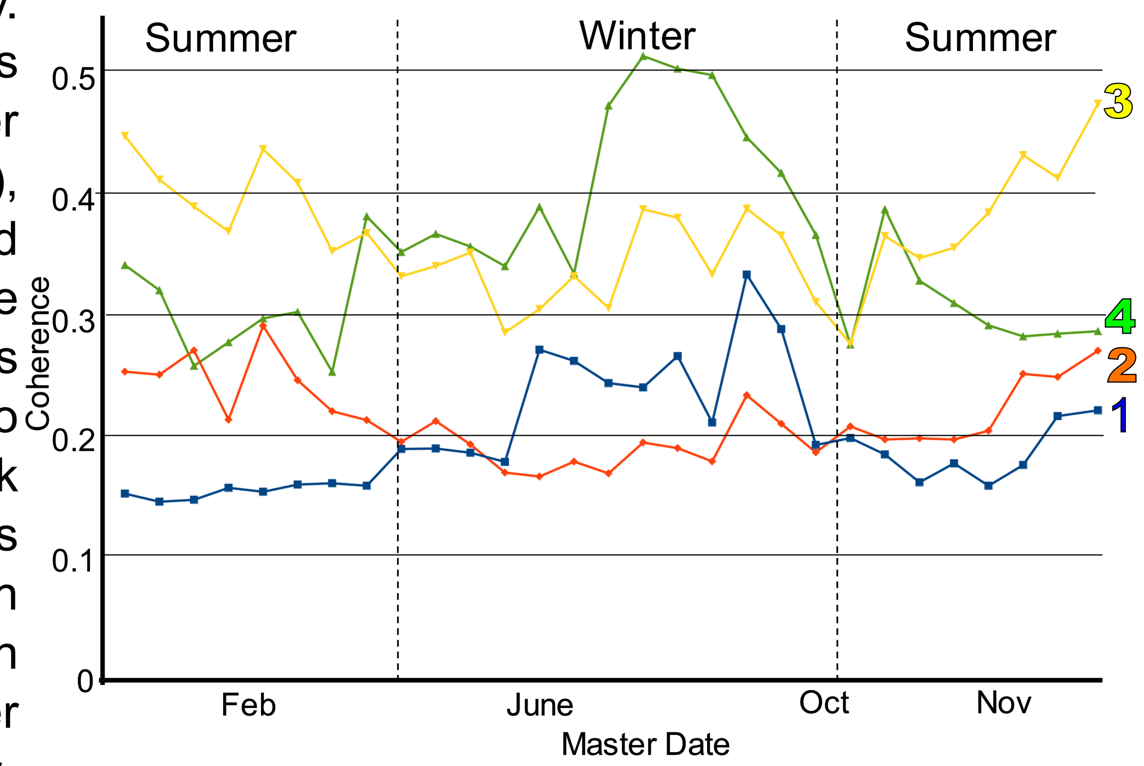

Fig 4) The average coherence over the Southern Alps was found for every combination of interferograms from 20170101-20190220 (2177 IFGs), and are displayed in a coherence matrix, where the shortest temporal baselines are on the diagonal. Results are then filtered to remove those dates that do not exceed and average coherence above a threshold of 0.15. This left 150 coherent interferogram combinations that can be used. The 4 interferograms circled meet the coherence threshold, but cannot be connected back to the rest of the network, so were not included in later StaMPS/MTI processing.

Inset: Full coherence matrix without threshold applied, demonstrating the seasonal effect on coherence.

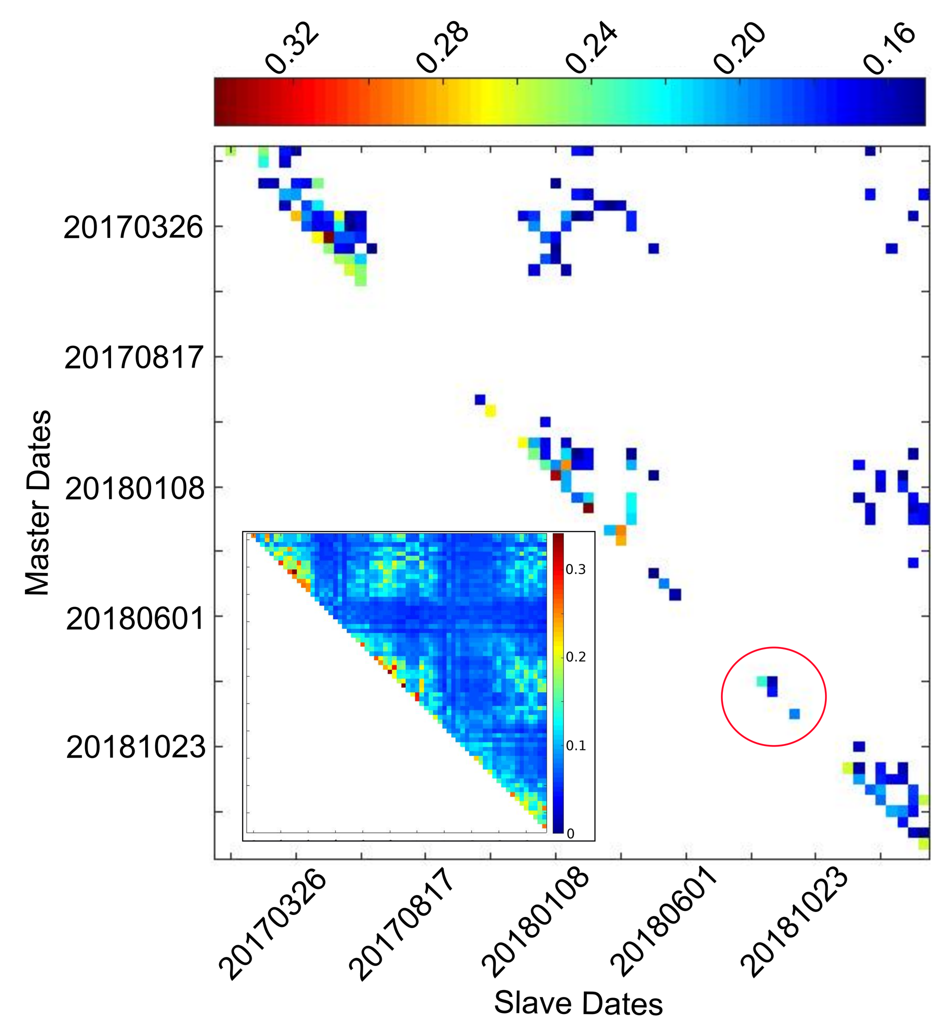

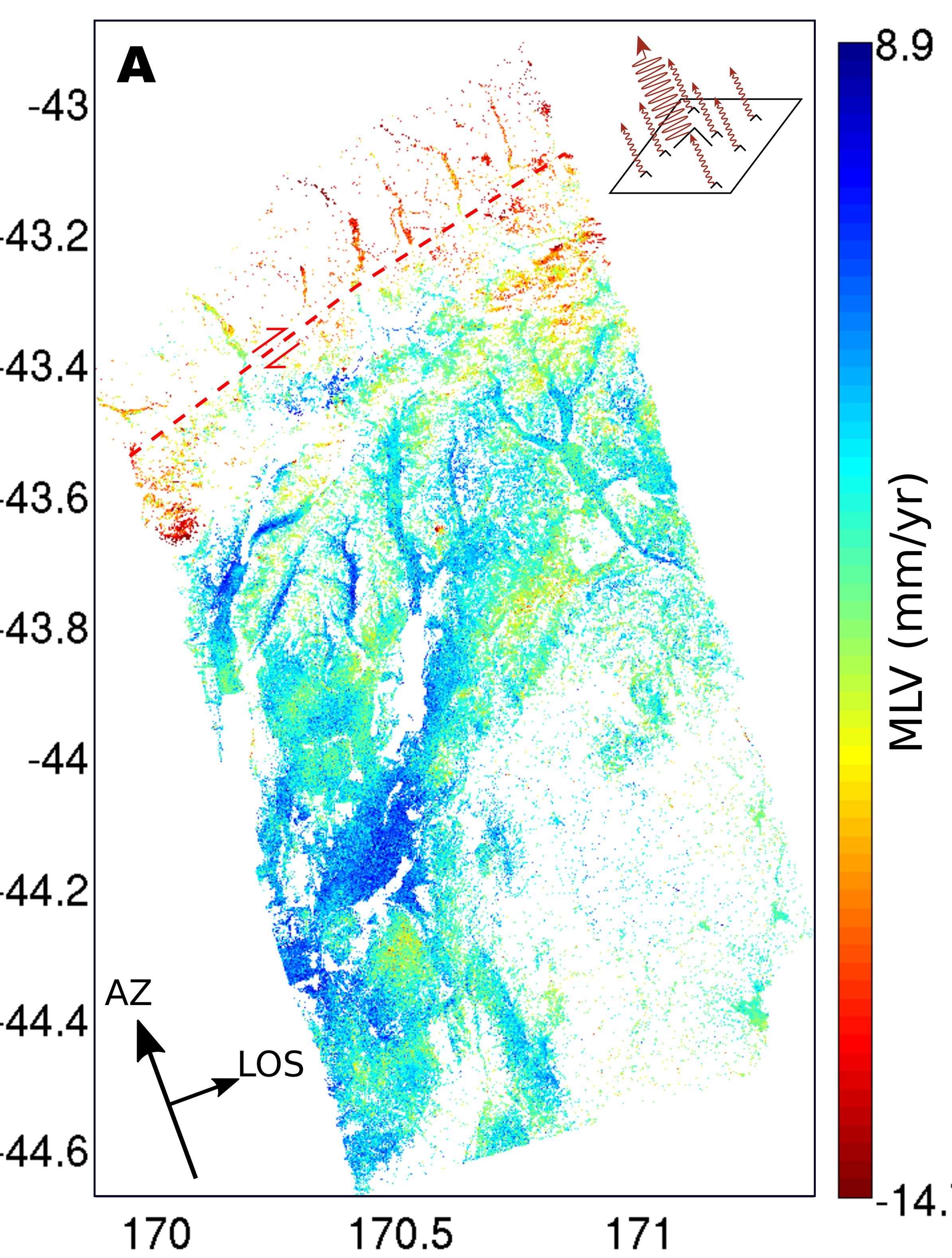

Fig 5) By using the StaMPS/MTI processing algorithm, it is possible to detect a signal, and therefore invert for a velocity, from much closer to the AF than by utilising a cumulative displacement from an interferogram chain. It does this by implementing a persistent scatterer (PS) method (A) with a small baseline (SB) approach (B) on full resolution interferograms. Pixels selected by each method will later be merged to form a single integrated dataset. Velocity maps cover the area highlighted in Fig 2, with positive being movement towards LOS

(C) A network diagram showing the SB connections used (green lines). All acquisitions (empty circles) were co-registered to a single master (filled circle). PS pixels were selected from interferograms formed from the single master

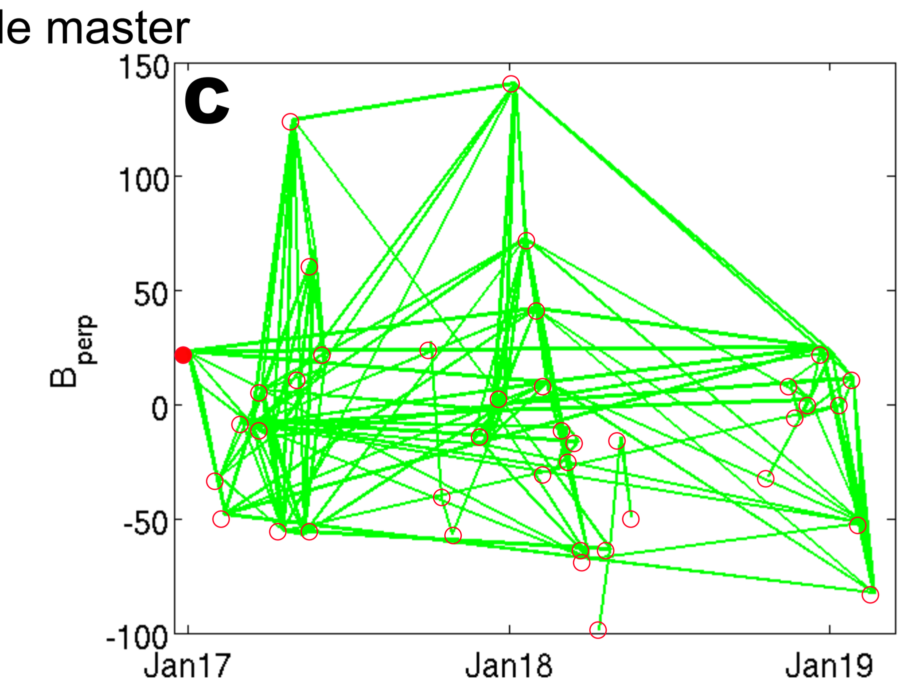

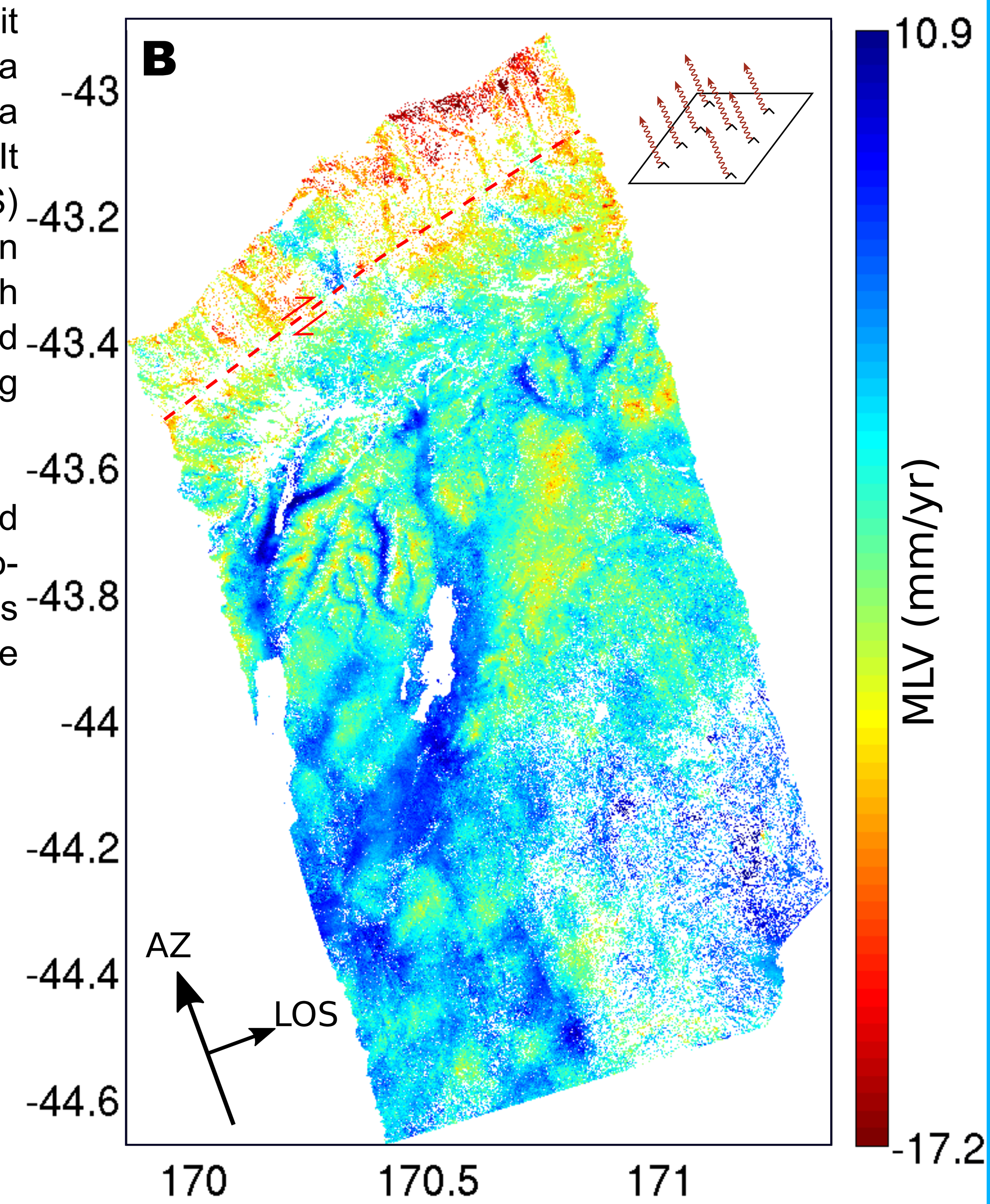

Beavan, J; Wallace, L; Palmer, N; Denys, P; Ellis, S; Fournier, N; Hreinsdottir, S; Pearson, C; Denham, M; (2016), New Zealand GPS velocity field: 1995-2013, New Zealand Journal of Geology and Geophysics, 59, 5-14.
González, PJ; Walters, RJ; Hatton, EL; Spaans, K; McDougall, A; Hooper, AJ; Wright, TJ; (2016), LiCSAR: Tools for automated generation of Sentinel-1 frame interferograms, AGU Fall Meeting
Hooper A; Bekaert D; Spaans K; Arikan M (2012), Recent advances in SAR interferometry time series analysis for measuring crustal deformation, Tectonophysics, 514-517, pp.1-13.
Werner, C; U. Wegmuller, U; Strozzi, T; Wiesmann, A; (2000), Gamma SAR and interferometric processing software, in Proceedings of the ERS-Envisat Symposium, Gothenburg, Sweden, vol. 1620, p. 1620